Electronic Supplementary Material (ESI) for Dalton Transactions.

Supporting information

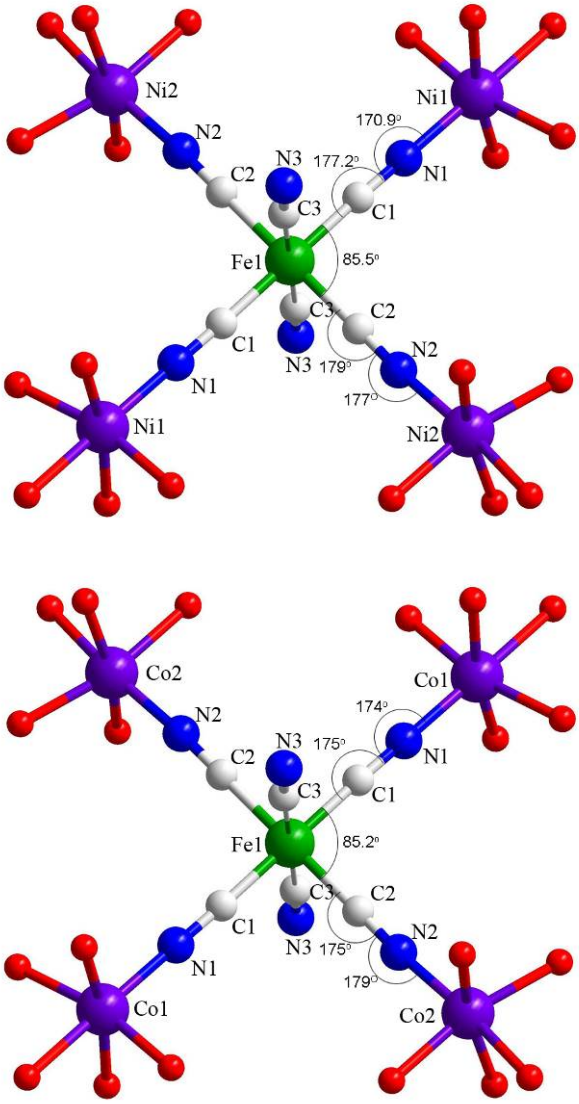

Fig. S1. ball-and-stick representation of the $[Fe^{III}_2Mn^{II}_2Fe(CN)_6]$ unit in **1**(top) and **2** (down) (O-red).

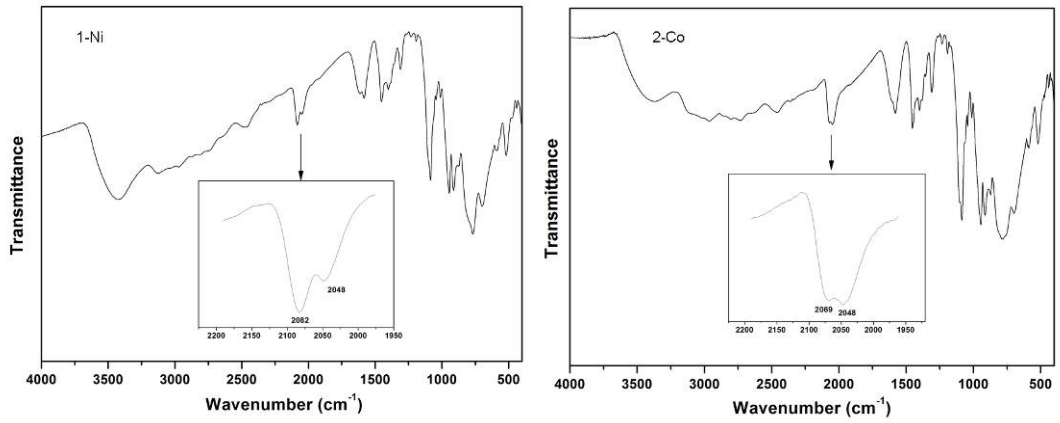

Fig. S2 IR of spectra of **1** and **2**

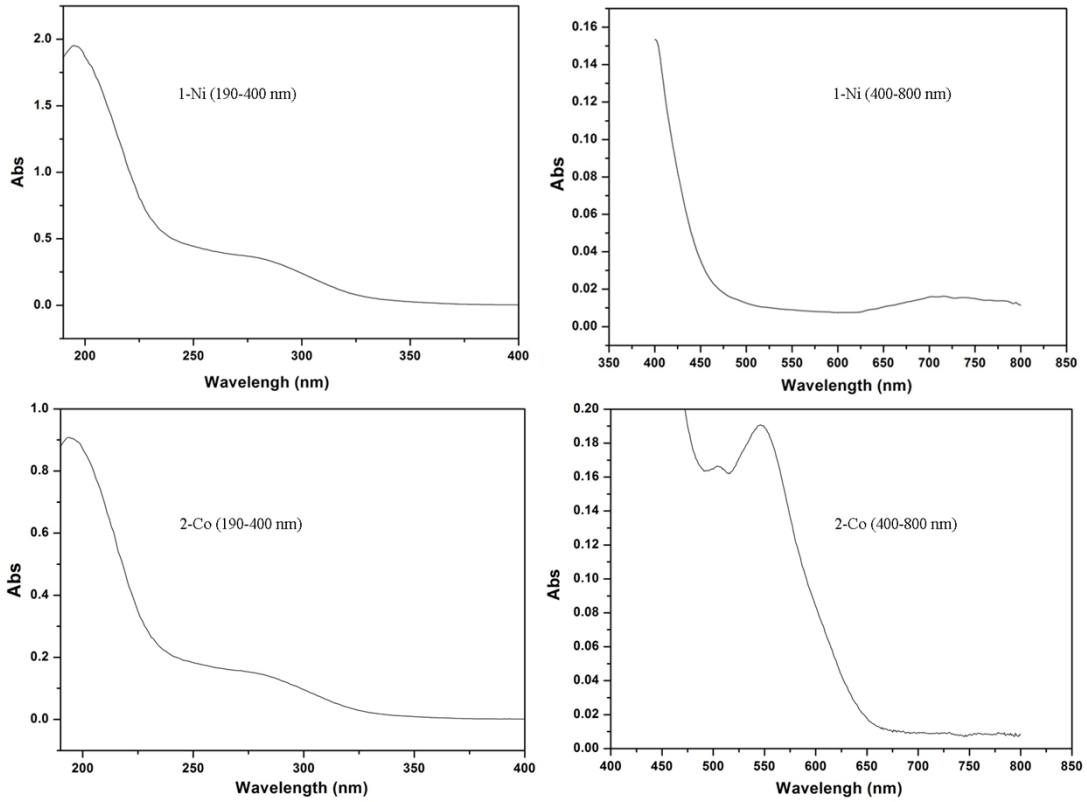

Fig. S3. Electronic absorption spectra of **1** and **2.** Two absorption bands at 195 nm, 287 nm for **1** and 194 nm, 282 nm for **2** is assigned to the charge transfer transition of $O_t \rightarrow Mo$ and $O_{b,c} \rightarrow Mo$. The peaks at 720 nm for **1** and 546 nm for **2** are assigned to transition metal ions to POM ligand charge transfer.

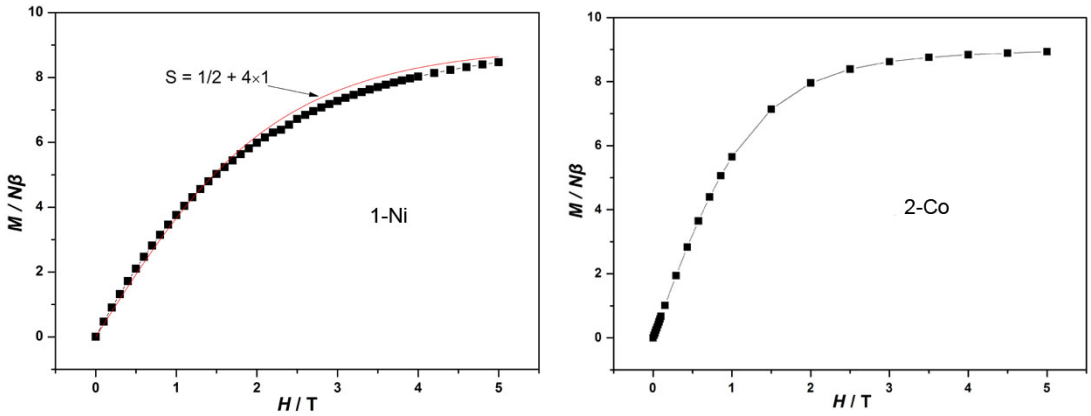

Fig. S4. Field dependence of magnetization of **1** (left) and **2** (right) at 2 K. For **1**, the solid line represents the Brillouin function that corresponds to non-interacting S = $1\times S_{Fe} + 4\times S_{Ni}$ with $g = 2.0$.

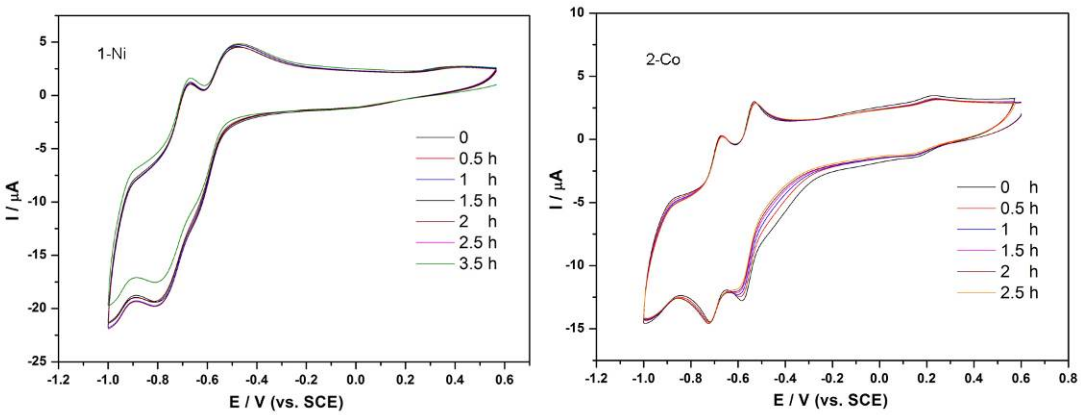

Fig. S5. Cyclic voltammograms of compounds **1**and **2** in 0.2 M NaH_2PO_4-Na_2HPO_4 buffer solution (pH = 6.2) taken at different times.

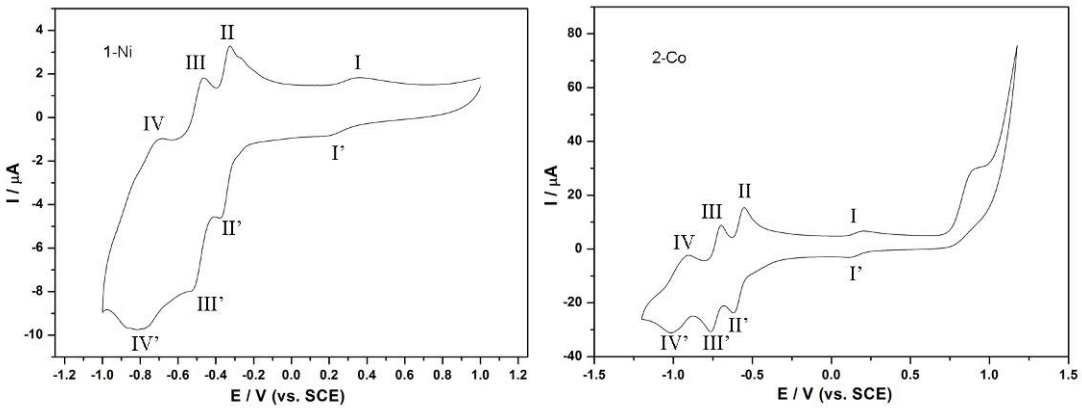

Fig. S6. Cyclic voltammograms of compounds **1**and **2** in 0.2 M NaH_2PO_4-Na_2HPO_4 buffer solution (pH = 6.2) at a scan rate of 50 mV/s

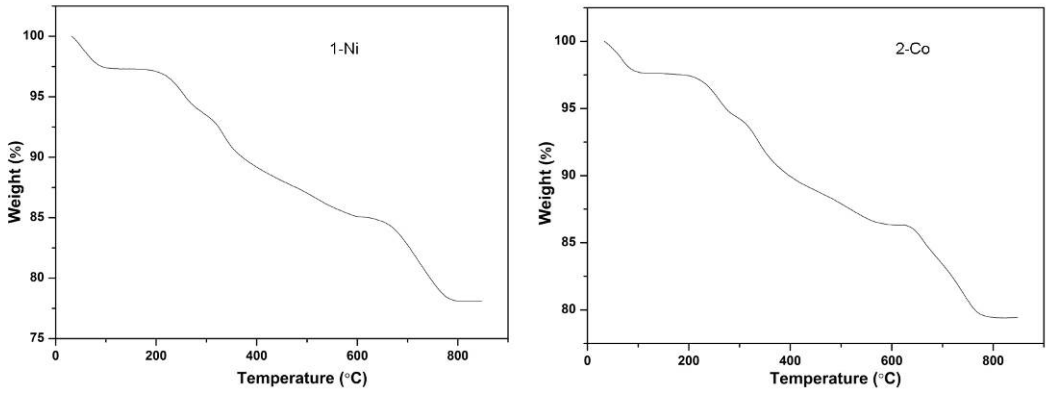

Fig. S7. The TG curve of complex **1** and **2.**

For **1**, it shows three steps of weight loss. The first loss of 2.69% (calc 2.62%) in the temperature range of 33-129 ^{o}C, could be assigned to the loss of lattice water. The second and third weight loss of 19.09% (calc 17.95%) in the temperature range of 164-800 ^{o}C, corresponds to the loss of organic moieties, together with the decompostition of $[Ni^{II}_4Fe^{III}(CN)_6]^{5+}$ fragment. For **2**, in the temperature range of 31.5-115.5 ^{o}C, the first loss of 2.38% (calc 2.30%) is assigned to the loss of lattice water. The second and third weight loss of 18.20% (calc 17.43%) in the temperature range of 178-805.5 ^{o}C could be ascribed of the loss of organic moieties, the decompostition of $[Co^{II}_4Fe^{III}(CN)_6]^{5+}$ fragment.

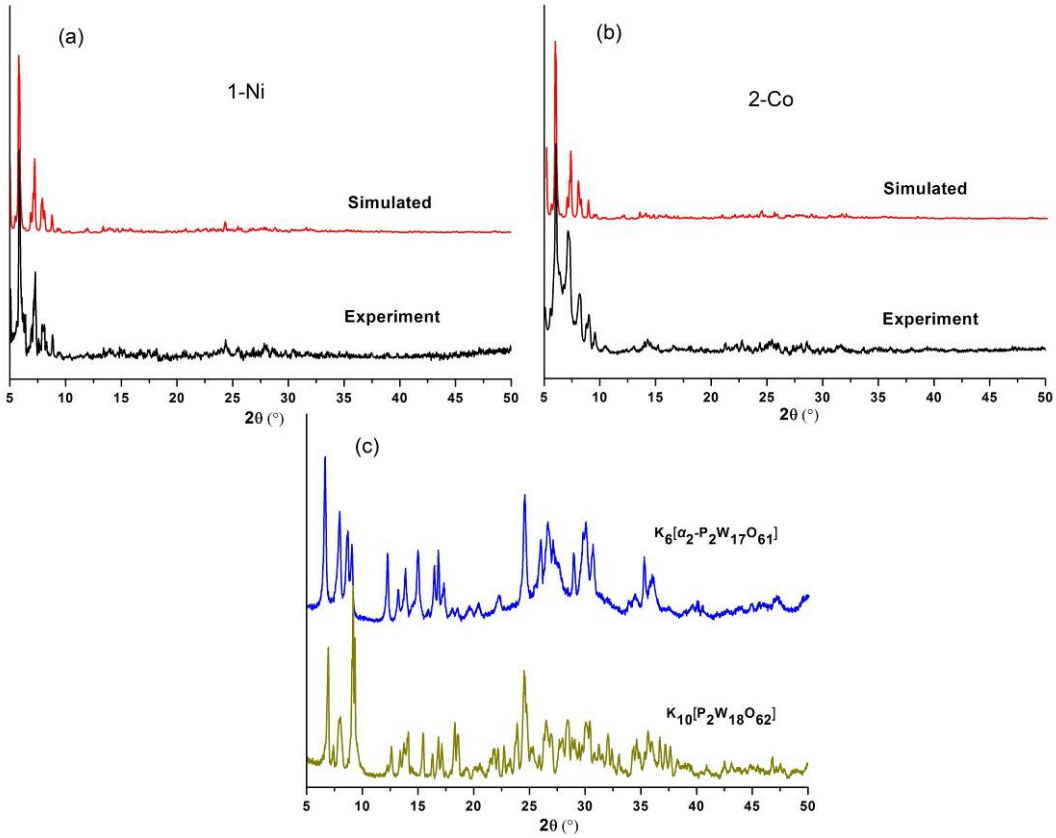

Fig. S8. Powder XRD pattern of **1** (a) and **2** (b) (black line) and simulated powder XRD pattern from data collected from a single crystal of **1** and **2** (red line) through the program 'Mercury'. (c) Powder XRD pattern of the material $K_6[P_2W_{18}O_{62}]$ and $K_{10}[\alpha_2\text{-}P_2W_{17}O_{61}]$. The experimental XRD patterns are in good agreement with the simulated XRD patterns, demonstrating the good phase purity for **1** and **2**. The differences in intensity between the experimental and simulated XRD patterns might be due to the variation in preferred orientation of the powder sample during collection of the experimental XRD.[1]

[1] J. Wang, J. W. Zhao, H. Y. Zhao, B. F. Yang, H. He and G. Y. Yang, *CrystEngComm*, 2014, **16**, 252-259.

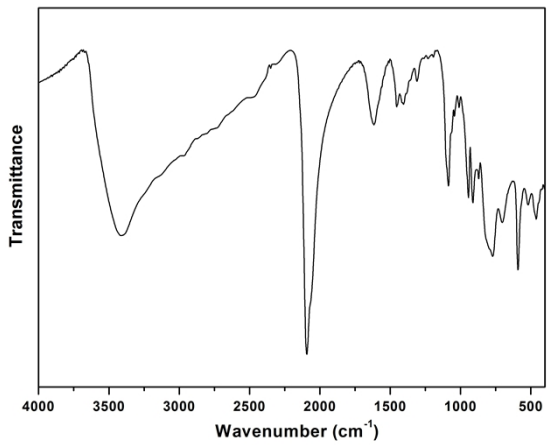

Fig. S9. The IR of the precipitate formed after the reactants were mixed, which are

proved to be a mixture of Prussian blue analogues and mono-metal-substituted POMs ($[P_2W_{17}MO_{61}]^{8-}$). These by-products result in the low yields of **1** and **2**.

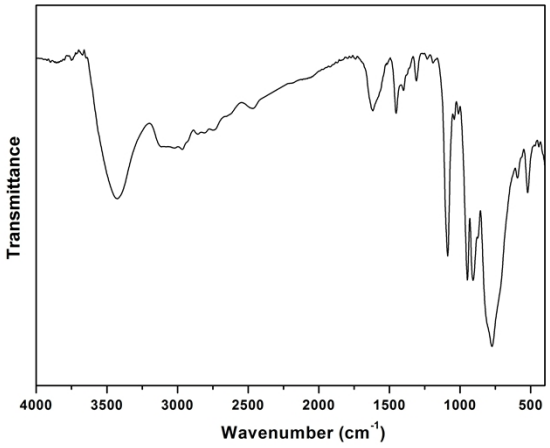

Fig. S10. The IR of the by-produce powders of mono-metal-substituted POMs without cyanometalate linker ($[P_2W_{17}MO_{61}]^{8-}$). The reaction solution was stilly evaporated at room temperature after no target produce being isolated and the powder of by-produce was formed.